Chemical structure regulates the formation of secondary organic aerosol and brown carbon in nitrate radical oxidation of pyrrole and methylpyrroles

Raphael Mayorga[1], Kunpeng Chen[2], Nilofar Raeofy[2], Megan Woods[1], Michael Lum[2], Zixu Zhao[1,a], Wen Zhang[1], Roya Bahreini[1,2,3], Ying-Hsuan Lin[2,3], Haofei Zhang[1,2,3*]

[1]Department of Chemistry, University of California, Riverside, CA 92507, USA

[2]Department of Environmental Sciences, University of California, Riverside, CA 92507, USA

[3]Environmental Toxicology Graduate Program, University of California, Riverside, CA 92507, USA

[a]Present address: Department of Environmental Sciences, Policy, and Management, University of California, Berkeley, CA 94720, USA

[*]Corresponding Author.

E-mail address: haofei.zhang@ucr.edu (H. Zhang).

Abstract:

Nitrogen-containing heterocyclic volatile organic compounds (VOCs) are important components of wildfire emissions that are readily reactive towards nitrate radicals (NO_3) during nighttime, but the oxidation mechanism and the potential formation of secondary organic aerosol (SOA) and brown carbon (BrC) are unclear. Here, NO_3 oxidation of three nitrogen-containing heterocyclic VOCs: pyrrole, 1-methylyrrole (1-MP), and 2-methylpyrrole (2-MP) were investigated in chamber experiments to determine the effect of precursor structures on SOA and BrC formation. The SOA chemical compositions and the optical properties were analyzed using a suite of online and offline instrumentation. Dinitro- and trinitro-products were found to be the dominant SOA constituents from pyrrole and 2-MP, but not observed from 1-MP. Further, the SOA from 2-MP and pyrrole showed strong light absorption while that from 1-MP were mostly scattering. From these results, we propose that NO_3-initiated hydrogen abstraction from the 1-position in pyrrole and 2-MP followed by radical shift and NO_2 addition leads to the light-absorbing nitroaromatic products. In the absence of a 1-position hydrogen, NO_3 addition likely dominates the 1-MP chemistry. We also estimate that the total SOA mass and light absorption from pyrrole and 2-MP are comparable to those from phenolic VOCs and toluene in biomass burning, underscoring the importance of considering nighttime oxidation of pyrrole and methylpyrroles in air quality and climate models.

Keywords: Biomass burning, light absorption, heterocyclic VOC, nitroaromatics, organic nitrate

Synopsis: Pyrrole and 2-methylpyrrole emitted from biomass burning may largely form nitroaromatic products with strong light absorption during nighttime nitrate radical oxidation through hydrogen abstraction of the secondary amine functional groups.

TOC:

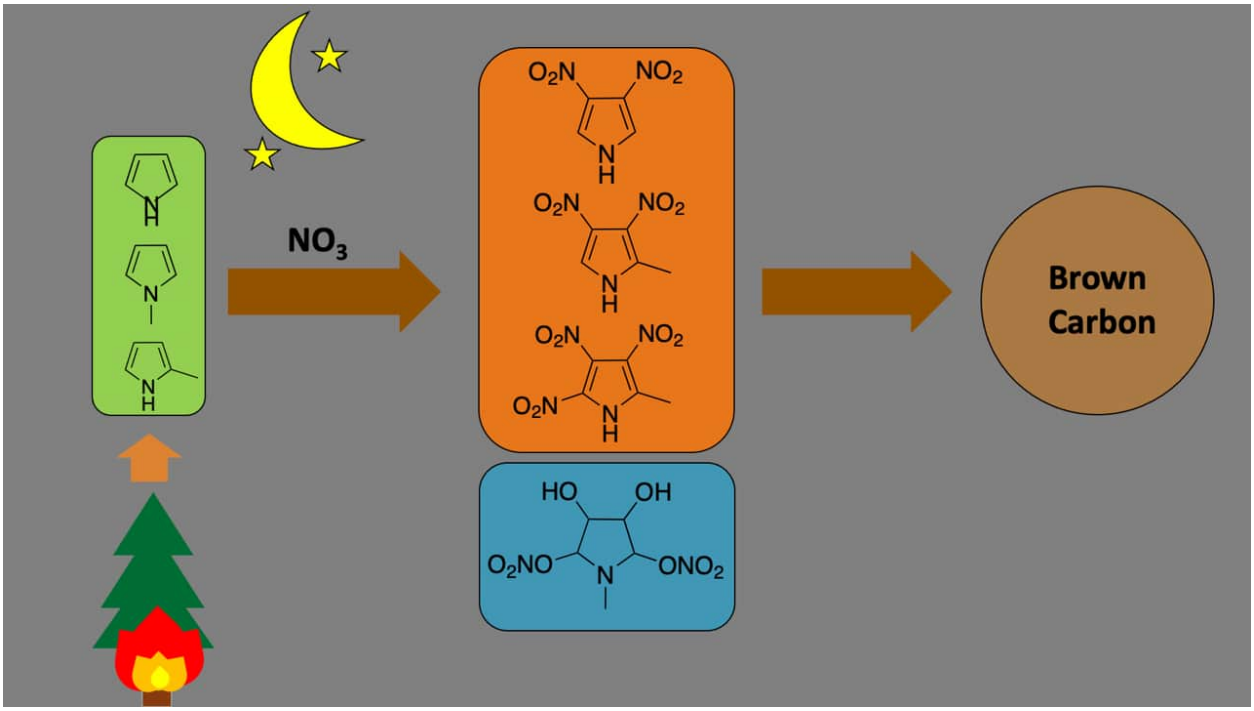

Introduction

In recent years, wildfires have shown a global increase in occurrence and severity.[1,2] Biomass burning events release volatile organic compounds (VOCs) and particulate matter into the atmosphere which impact the Earth's radiative budget, air quality and human health.[3,4] Nitrogen-containing heterocyclic VOCs such as pyrrole and its methyl derivatives could represent an important portion of wildfire emissions. From fuels native to North America, pyrrole has emission factors ranging from 0.014 – 0.11 g kg^{-1}, 1-methylpyrrole (1-MP) from 0.0023 – 0.023 g kg^{-1} and 2-methylpyrrole (2-MP) from 0.0023 – 0.015 g kg^{-1}.[5,6] In comparison, another class of well-studied wildfire emissions, phenolic VOCs, have total emission factors ranging from 0.10 – 0.64 g kg^{-1} from similar fuels.[7–9] During biomass burning events, increased levels of NO_x (= NO + NO_2) can quickly react with ozone (O_3) to produce nitrate radicals (NO_3), which may act as the primary oxidant for some VOCs during nighttime,[10–12] and even during daytime.[13] The NO_3 oxidation of pyrrole and methylpyrroles has been understudied but may represent a significant pathway towards the formation of secondary organic aerosol (SOA).[14] These SOA are often found to be light absorbing (i.e., forming brown carbon, BrC), which further enhance their climate impacts.[15–17] Therefore, it is of vital importance to understand the NO_3 oxidation chemistry of pyrrole and methylpyrroles and incorporate it into the current air quality and climate models.

Several prior studies have investigated NO_3 oxidation of heterocyclic VOCs such as furan and methylfurans,[18–20] but there have been very few studies of pyrrole and methylpyrroles.[14,21] The primary nighttime oxidant, NO_3, has been shown to react very quickly with pyrrole in the gas phase with a rate constant of 4.9×10^{-11} cm^3 $molecules^{-1}$ s^{-1}.[22,23] The low-volatile products from NO_3 oxidation of pyrrole can partition into the particle phase with significant SOA yields and exhibit strong light-absorbing properties.[14] Pyrrole has been reported to have 109 ± 29% SOA

yield from NO_3 oxidation and an average mass absorption coefficient (<MAC>) of 0.34 ± 0.07 m^2 g^{-1} from 290 – 700 nm encompassing the UV and visible light.[14] However, the composition and formation mechanism of SOA and BrC from NO_3 oxidation of pyrrole and methylpyrroles remain poorly understood. Pyrrole and methylpyrroles contain double bonds which might undergo NO_3 addition following mechanisms like those established for many alkenes to form organic nitrates;[24–29] they are also aromatic compounds, thus it is conceivable that they could also undergo reactions involving H-abstraction by NO_3 like those reported for phenolic VOCs and form nitroaromatics in the presence of NO_2.[30–35] In the NO_3 oxidation of phenolic VOCs, nitroaromatic products generally constituted a significant portion of SOA mass and may contribute to the strong light absorption.[30,32,33,36–39] In this study, we investigate the SOA formation from NO_3 oxidation of pyrrole, 1-MP and 2-MP using a comprehensive suite of analytical instrumentation. We identify the major SOA products from NO_3 oxidation of the three N-containing heterocyclic VOCs, measure the optical properties of their SOA, and discuss how the chemical structure regulates the oxidation mechanisms that lead to the distinct formation of light-absorbing chromophores.

Materials and Methods

Chemicals and reagents. The chemicals and reagents used in this study and their purities and suppliers are as follows: pyrrole (TCI America, >99%), 1-methylpyrrole (TCI America, >99%), 2-methylpyrrole (aa blocks, 98%), sodium chloride (99.5%, Sigma Aldrich), methanol (HPLC Grade Fischer Chemical), and acetonitrile (HPLC Grade Fischer Chemical). All chemicals were used without further purification.

Laboratory experiments. All the experiments (see **Table 1**) were performed in a 10 m^3 Teflon FEP smog chamber under dark conditions, low relative humidity (RH < 20%), at room

temperature (20 – 25°C) and pressure (730 Torr). A duplicate experiment was performed for each of the five conditions listed in **Table 1** to verify reproducibility. NO_3 radicals were generated through the reaction of O_3 and NO_2 in the chamber. O_3 was introduced into the chamber using an O_3 generator (A2Z Ozone 3GLAB) and the initial concentration of O_3 for each experiment was ~ 1400 – 1700 ppb. Directly following this, NO_2 (Airgas) was injected into the chamber to achieve an NO_2 concentration of ~ 150 ppb or 450 ppb. Thus, the initial NO_2/O_3 ratio in the chamber was approximately 0.1 or 0.3, which is similar to that measured in relatively fresh wildfire plumes.[40] The O_3 and NO_x concentrations in the chamber were measured in real-time by an O_3 analyzer (Advanced Pollution Instrumentation, Inc.) and a NO_x analyzer (Teledyne Instruments), respectively. O_3 and NO_2 were allowed to react for ~ 1 h in the chamber before injection of pyrrole, 1-MP, or 2-MP at approximately 200 ppb by passing 15 L min^{-1} of N_2 gas through a heated jar containing the liquid VOC to initiate the NO_3 oxidation experiment. A scanning electrical mobility scanner and a mixing condensation particle counter (SEMS and MCPC, Brechtel Manufacturing Inc.) were used to measure size distribution and number concentrations of the SOA from 10 – 800 nm with 140 size bins. After the formed SOA mass concentrations reached a plateau, SOA samples were collected on PTFE membrane filters (Tisch Scientific) at 16.7 L min^{-1} for 1 h, allowing for a total collected SOA mass of 149 – 422 μg, estimated based on the measured aerosol effective densities described below. The collected SOA samples were stored at -20°C until analysis. Before all the aerosol measurements, the particles from the chamber passed through a 30 cm-long diffusion dryer filled with silica gel (Sigma-Aldrich) and Purafil (Thermo Scientific).

In addition to the chamber experiments, we also performed kinetic experiments in a continuous flow stirred tank reactor (CFSTR) to constrain the oxidation rate constants of 1-MP and 2-MP in reactions with O_3 and NO_3 radicals.[35,41] The decays of the methylpyrroles relative to

pyrrole upon oxidation by O_3 and NO_3 radicals were measured by a proton-transfer reaction mass spectrometer (PTR-MS). Details are described in the **Supplemental Information (SI), Text S1.**

***SOA Chemical Characterization*.** The collected SOA filter samples were extracted for offline chemical analysis. Specifically, 20 mL of methanol was added to each vial containing a filter sample followed by 45-min sonication. The filters were then removed from the vials and methanol was evaporated off with a gentle flow of N_2. Immediately after filter extraction, the extracts were dissolved in 100 μL acetonitrile with 0.1 mM NaCl for analysis using an electrospray ionization (ESI) ion mobility spectrometry time-of-flight mass spectrometer (IMS-TOF, Tofwerk Inc.) in the negative ion mode. The doped NaCl allows for molecules to form adducts with chloride $[M+Cl]^-$ in (–)ESI, which has been shown to be an effective approach to detect non-acidic organic nitrates which are otherwise challenging to ionize directly by ESI.[42] Each sample extract was injected into the IMS-TOF using a syringe pump at a rate of 1 μL min^{-1}. After the (–)ESI, the generated ions enter into a drift tube and are met with a counterflow of N_2 gas (at 1.2 L min^{-1}) which serves to separate different ions based on their collisional cross sections thereby giving each ion a characteristic drift time.[35,43] Upon exiting the drift tube, the ions were focused through a pressure-vacuum interface which contains two segmented quadrupoles operated at ~ 2 mbar and 5 × 10^{-3} mbar, respectively. By varying the voltages between the two segmented quadrupoles, collision-induced dissociation (CID) of parent ions is achieved. The IMS-TOF was operated over an m/Q range of 45 – 600 Th. The IMS resolution is $(t/\Delta t) \sim 100$ and the TOF mass resolution is $(m/\Delta m) \sim 4000$, determined by various standard ions with m/Q between 100 – 200 Th.[35,42] All the IMS-TOF data processing were performed using Tofware (version 3.2.0, Tofwerk Inc.) running with Igor Pro (Wavemetrics Inc.).[35,44]

In addition, size-resolved mass distributions and particle chemical composition were measured in real-time by a mini aerosol mass spectrometer (mAMS) coupled with a compact time-of-flight mass spectrometer (Aerodyne Research, Inc.).[45] The size-resolved aerosol mass distribution was compared with the concurrent SEMS-derived aerosol volume distribution to determine the effective aerosol density (ρ_{eff}).[45–47] The calculation of ρ_{eff} is described in the **SI, Text S2**. The calculated ρ_{eff} was then used to estimate the SOA mass concentrations shown in **Table 1**. The mass accuracy of the mAMS is ~ 20 ppm and the resolving power is ~ 1200 – 1300. Size selected ammonium nitrate particles or dry polystyrene latex spheres were regularly used to calibrate the sensitivity and sizing capability of the mAMS. High resolution analysis of the raw mass spectra was conducted from *m/Q* 20 – 115 Th to calculate the mass concentrations of all species.[48] Besides, supportive gas-phase chemical analysis was performed for selected experiments (pyrrole and 1-MP) with a chemical ionization mass spectrometer using iodide (I^-) as the reagent ion (I-CIMS, Aerodyne Research Inc.). The I^- forms adducts ($[M + I]^-$) with functionalized molecules containing oxygens and nitrogens. Further details about this instrument can be found in our previous publication.[14]

SOA Optical Property Characterization. Online analysis of the SOA optical properties was performed using a Photoacoustic Extinctiometer (PAX, Droplet Measurement Technology, Boulder, CO). The PAX allows for measurements of absorption and scattering coefficients at 375 nm ($\beta_{abs,375}$ and $\beta_{scat,375}$) at 1 Hz, which were averaged to the SEMS scan time interval (140 s).[14] Online <MAC> at 375 nm ($<MAC>_{online,375}$) was estimated by:

$$MAC_{online,375} = \frac{\beta_{abs,375}}{C_{SOA}} \quad (1)$$

where C_{SOA} is the estimated SOA mass concentration. The calculation of C_{SOA} is described in the **SI**, **Text S2**. The single scattering albedo (SSA) at 375 nm was calculated by:

$$SSA_{375} = \frac{\beta_{scat,375}}{\beta_{scat,375} + \beta_{abs,375}} \quad (2)$$

The calculated SSA is size dependent and is calculated as a function of size parameter (α). α was determined with the following equation using d_m and the wavelength of radiation used in PAX (λ = 375 nm):[46]

$$\alpha_{375} = \frac{\pi d_m}{\lambda} \quad (3)$$

Offline <MAC> profiles were obtained using measurements from a UV-Vis spectrophotometer (Beckman DU-640). All the UV-Vis spectroscopy measurements were operated under 293 K and 1 atm.[14] The SOA filter samples were extracted using acetonitrile as the solvent, following the same extraction procedure as described above. The data from these measurements were used to calculate the <*MAC*> in $m^2\ g^{-1}$ for each sample:

$$< MAC >_{offline} = \frac{A(\lambda) \times \ln(10)}{b \times C_m} \quad (4)$$

where *A(λ)* is the absorbance at the wavelength of interest, *b* is path length of cuvette (0.01 m) and C_m is the concentration of SOA in $g\ m^{-3}$.[14] Additionally, the absorption Angström exponent (*AAE*) was calculated for each <MAC> profile from this data:

$$AAE_{\frac{\lambda_1}{\lambda_2}} = \frac{-\ln \frac{< MAC > (\lambda_1)}{< MAC > (\lambda_2)}}{\ln(\frac{\lambda_1}{\lambda_2})} \quad (5)$$

where λ_1 and λ_2 are two selected wavelengths. $AAE_{290/400}$ and $AAE_{400/600}$ were calculated, which will improve our understanding of the wavelength dependence of light absorption in the UV (290 – 400 nm) and visible (400 – 600 nm) regions.[14]

In addition, offline analysis of chemical composition and light absorption was also carried out using liquid chromatography coupled (LC) with a diode array detector (DAD) and (–)ESI high resolution time of flight mass spectrometer ((–)ESI-HR-TOFMS, Agilent 6545 series).[14]

Kinetic simulations for NO_3 concentrations and TD-DFT calculations. In this work, since direct NO_3 measurement was unavailable, a kinetic model was used to estimate the concentrations of NO_3 before VOC injection for each experiment based on the measured initial O_3 and NO_2 concentrations.[49] The gas-phase loss of NO_3 and N_2O_5 to the Teflon wall are incorporated into the simulations using rates reported in previous research.[50] The model suggests that NO_3 concentrations stabilized at ~8.0 ppb and ~22.0 ppb for NO_x/O_3 ratios of 0.1 and 0.3, respectively before VOC injections. The kinetic model was also used to estimate the fractions of VOCs oxidized by NO_3 vs. O_3 using reaction rates reported in previous literature (for pyrrole)[22] and constrained in the CFSTR experiments in this work (for the methylpyrroles). As described in the **SI**, **Text S1**, 1-MP reacts with O_3 faster than pyrrole by a factor of ~ 3.3 and with NO_3 slower than pyrrole by a factor of ~ 1.9. In contrast, 2-MP reacts faster with both O_3 and NO_3 than pyrrole by a factor of ~ 10.3 and ~ 9.8, respectively. Despite the variations in their reactivities, over 92% of all three VOCs was oxidized by NO_3 under the chamber conditions based on the kinetic model, suggesting the dominance of NO_3 oxidation chemistry in the SOA formation.

In addition, time-dependent density functional theory (TD-DFT) computational chemistry approaches were also used in this study to predict the UV-Vis spectra for several BrC chromophores of interest.[51] The calculations for the predicted UV-Vis spectra were performed with the Gaussian 16 program and the spectra were visualized using GaussView 06 software. All calculations were computed with acetonitrile as the solvent to be consistent with the offline UV-Vis measurements. To optimize the geometry PBE0 functional method with the 6-311+G(d,p) basis set was used, along with acetonitrile as the solvent. Likewise, the same functional method and basis set were used for the TD-DFT calculations, with 20 excited states. The cartesian

198 coordinates for optimized geometries used for the simulated UV-Vis spectra are listed in **Tables**
199 **S1-S2**.
200
201 **Results and Discussion**
202 ***Chemical Composition of the SOA*. Figure 1** presents the (–)ESI-IMS-TOF mass spectra
203 for SOA from NO_3 oxidation of pyrrole, 2-MP and 1-MP in the experiments with initial NO_2/O_3
204 = 0.3, with chemical formulas highlighted for the major product ions. Similar mass spectra from
205 the initial NO_2/O_3 = 0.1 experiments are shown in the **SI, Figure S1**. All the identified major ions
206 contain at least two nitrogen atoms and have $[M\text{-}H]^-$ chemical formulas, despite the usage of NaCl
207 as the dopant. This deprotonation ionization scheme was previously reported for nitroaromatics
208 and nitrophenols using the same instrument.[35,42,52] In contrast, non-acidic organic nitrates were
209 found to mainly form $[M+Cl]^-$ adducts with doped Cl^-.[42] Alternatively, organic nitrates containing
210 acidic groups may also exhibit $[M\text{-}H]^-$. The acidic groups could be carboxylic acids or alcohols on
211 heterocyclic rings.[53] To distinguish between nitroaromatics and acidic organic nitrates (which may
212 also deprotonate by the acidic groups in (–)ESI), we introduce a term for the three studied VOC
213 systems, "NO_x index":

214 $$I_{NOx} = \frac{n_O}{n_N - 1} \qquad (6)$$

215 where n_O and n_N are the numbers of oxygens and nitrogens per formula, respectively; $n_N - 1$
216 represents the number of additional nitrogens to the initial pyrrole or methylpyrroles. Thus, for
217 products which only contain nitro groups ($–NO_2$), I_{NOx} = 2. To form organic nitrates ($–ONO_2$)
218 through NO_3 addition to a double bond, another O-containing functional group must be added via
219 peroxy radical chemistry. Therefore, for organic nitrate products, $I_{NOx} \geq 4$. I_{NOx} between 2 and 4
220 likely suggests multifunctional species that contain both $–NO_2$ and $–ONO_2$.

Table 1. Summary of Experimental Conditions[a].

VOC	$[O_3]_{eq}$ (ppb)[b]	$[NO_x]_{eq}$ (ppb)[b]	Peak SOA mass conc. ($\mu g\ m^{-3}$)[c]	<MAC>$_{offline}$ ($m^2\ g^{-1}$) (375 nm and 290-700 nm average)[d]	$AAE_{290/400}$ and $AAE_{400/600}$	SSA_{375}[e]
Pyrrole	1332	265	298	0.35/0.21	4.98/6.23	0.80 ± 0.01
1-MP	1308	262	250	0.13/0.07	5.14/8.00	0.97 ± 0.00
2-MP	1392	177	422	0.69/0.35	4.72/8.83	0.76 ± 0.01
Pyrrole	908	88	149	0.23/0.13	4.46/5.18	0.80 ± 0.02
1-MP	898	76	175	0.16/0.08	4.88/7.02	0.97 ± 0.00

[a]A duplicate experiment was performed for each of the five conditions and the values reported in the table are averages of duplicates which usually vary within 10%; [b]Steady-state O_3 and NO_x concentrations measured before 200 ppb of VOC injection. Here, NO_2, NO_3, and N_2O_5 could be detected as NO_x; [c]Peak SOA mass was calculated using calculated effective SOA density for each experiment; [d]The 290 – 700 nm results for <MAC> are averaged values within the specific wavelength ranges; [e]The average SSA_{375} throughout the experiments when the size parameter was greater than 1.

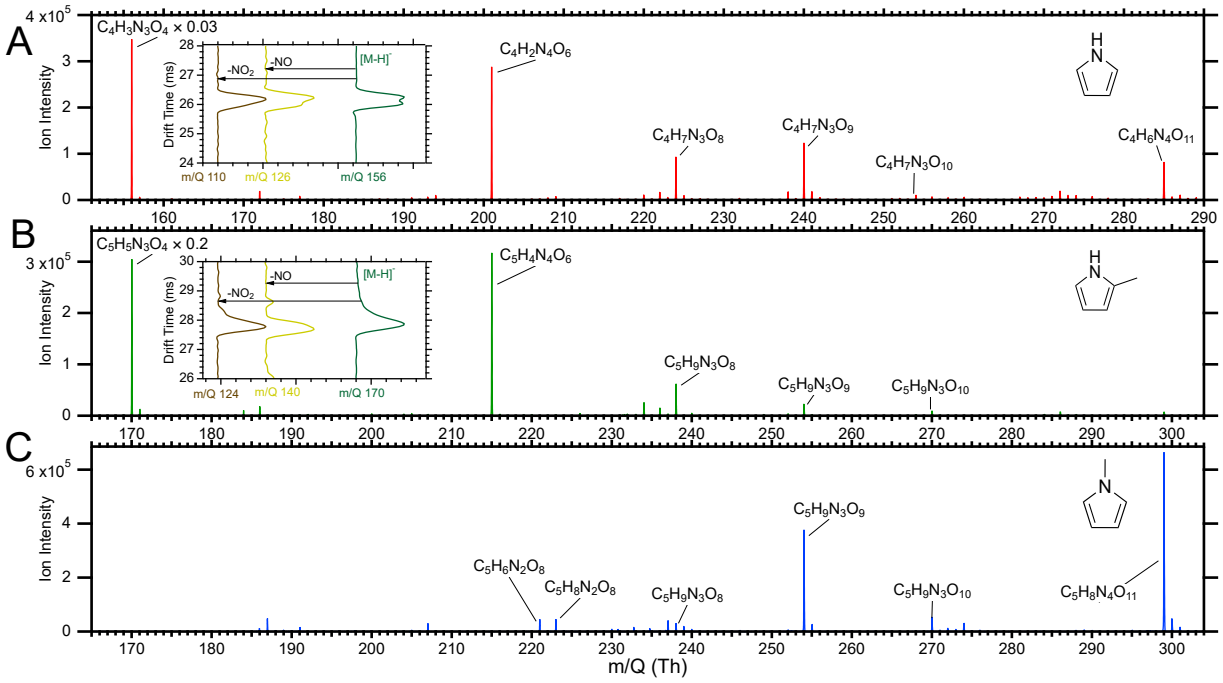

Figure 1. (–)ESI-IMS-TOF mass spectra with major products highlighted for (A) pyrrole + NO_3 SOA, (B) 2-MP + NO_3 SOA, and (C) 1-MP + NO_3 SOA. For simplicity, the molecular formulas are labeled. The intensities of significant products, $C_4H_3N_3O_4$ for pyrrole and $C_5H_5N_3O_4$ for 2-MP, are multiplied by factors of 0.03 and 0.2 respectively to make the additional key products visible. The inserted plots in (A) and (B) show characteristic fragment ions ($[M\text{-}H\text{-}NO]^-$ and $[M\text{-}H\text{-}NO_2]^-$) for $C_4H_3N_3O_4$ in pyrrole SOA and $C_5H_5N_3O_4$ in 2-MP SOA using IMS drift time vs. intensity data obtained at high CID voltage (20 V). The *x*-axes are shifted by +14 in (B) and (C) in comparison to (A), to account for the difference by $–CH_2$ in the VOC precursors, so that the oxidation products can be more easily compared.

From the NO_3 oxidation of pyrrole (**Figure 1A**) and 2-MP (**Figure 1B**), the most significant products identified in the SOA are $C_4H_3N_3O_4$ (*m/Q* 156 Th) and $C_5H_5N_3O_4$ (*m/Q* 170 Th), respectively. These formulas both have two additional nitrogens with $I_{NOx} = 2$, corresponding to dinitropyrrole and 2-methyl-dinitropyrrole, respectively. Following methods described in previous literature for identifying nitroaromatics in the IMS-TOF, we looked for the fragments of $[M\text{-}H\text{-}NO]^-$ and $[M\text{-}H\text{-}NO_2]^-$ at high CID voltage for these species which is indicative of the presence of $–NO_2$ functionality.[42] We found evidence of such fragments by identifying identical drift times between $[M\text{-}H]^-$, $[M\text{-}H\text{-}NO]^-$ and $[M\text{-}H\text{-}NO_2]^-$ for $C_4H_3N_3O_4$ in the pyrrole SOA and $C_5H_5N_3O_4$ in the 2-MP SOA (inserted plots in **Figure 1A** and **Figure 1B**), thereby confirming that they are dinitropyrrole and 2-methyl-dinitropyrrole, respectively. It should be mentioned that their ion intensities are 5 – 30 times higher than the second largest product ions and thus are the most important products in these oxidation systems. Similarly, the second largest products in the pyrrole and 2-methylpyrrole SOA are $C_4H_2N_4O_6$ (*m/Q* 201 Th) and $C_5H_4N_4O_6$ (*m/Q* 215 Th), which have

three additional nitrogens with I_{NOx} = 2, corresponding to trinitropyrrole and 2-methyl-trinitropyrrole, respectively. Although authentic standards are unavailable for quantification, prior work has shown that the relative sensitivities for SOA constituents in ESI-MS may vary by 1 – 2 orders of magnitude, and species with similar chemical structures and functional groups appear to have smaller variation.[54] Considering these factors, the dinitro- and trinitro-products are still major constituents in the SOA from pyrrole and 2-MP, clearly suggesting that these two heterocyclic VOCs exhibit a strong aromatic character during NO_3 oxidation and mainly form nitroaromatic products.

Strikingly, the SOA from 1-MP + NO_3 do not show the same behavior, despite the very similar chemical structure as pyrrole and 2-MP (**Figure 1C**). In fact, the same dinitro- and trinitro-products were not observed at all in 1-MP SOA. Instead, the main products in 1-MP SOA are $C_5H_9N_3O_{8\text{-}10}$ and $C_5H_8N_4O_{11}$. These products have I_{NOx} from 3.7 to 5, suggesting that they contain at least one –NO_3 with non-nitrogen-containing functional groups. Interestingly, similar high-I_{NOx} products were also observed in the SOA from pyrrole and 2-MP (**Figure 1A** and **1B**), but at much smaller intensities. These results strongly suggest that unlike pyrrole and 2-MP, 1-MP exhibits stronger alkene character which preferentially undergoes NO_3 addition. The molecular-level findings from the (–)ESI-IMS-TOF results were well supported by the complementary measurements using the LC-DAD-ESI-HR-TOFMS (**Figure S2**), where dinitropyrrole and 2-methyl-dinitropyrrole were found to be the most dominant products in the SOA from pyrrole and 2-MP, but no nitro-products were observed in the 1-MP SOA. In the measurements made by the mAMS, although the high vaporization temperature and ionization energy fragmented the molecular species into small ions and made product interpretation challenging, several characteristic fragment ions could still provide key evidence for the oxidation chemistry (**Figure**

277 **S3**). Specifically, both NO^+ (*m/Q* 30 Th) and NO_2^+ (*m/Q* 46 Th) are abundant in the mAMS mass
278 spectra, suggesting that nitro- or nitrate-containing products are major SOA constituents in all
279 three systems. Yet, distinct organic products and patterns are clearly shown. For example, when
280 comparing the SOA from 2-MP and 1-MP (which have the same VOC formulas), the 2-MP SOA
281 contain more fragment ions without oxygen (e.g., $C_3H_{2\text{-}3}^+$ and $C_{2\text{-}3}H_{0\text{-}3}N^+$), while the 1-MP SOA
282 have more fragment ions with oxygen (e.g., $C_2H_{2\text{-}4}NO^+$ and $CHNO_2^+$). Consistent with the
283 individual fragment ions, the 2-MP SOA have a higher fraction of the $C_xH_y^+$ family and the 1-MP
284 SOA have higher fractions of the $C_xH_yO_z^+$ and $C_xH_yO_zN^+$ families. These results imply that the 1-
285 MP SOA are likely comprised of more oxygen-containing functional groups with oxygens bonded
286 directly with carbons (e.g., –OH and $–ONO_2$) than the 2-MP SOA, agreeing with the molecular
287 composition results.

288 ***Optical properties of SOA***. To examine how the distinct functionalities in the SOA
289 compositions between pyrrole, 1-MP, and 2-MP discussed above may affect the SOA optical
290 properties, we report the light absorption and scattering properties by combing several online and
291 offline measurements. The results for online and offline optical properties from pyrrole, 1-MP and
292 2-MP SOA are tabulated in **Table 1**. In **Figure 2A**, the $<MAC>_{offline}$ is plotted as a function of
293 wavelength for SOA from NO_3 oxidation of pyrrole, 1-MP, and 2-MP. Here, the 2-MP SOA
294 showed to be the most absorbing with the highest $<MAC>_{offline}$, followed by the pyrrole SOA. In
295 contrast, the 1-MP SOA exhibited the least light absorbance with the lowest $<MAC>_{offline}$. These
296 $<MAC>_{offline}$ profiles suggest that the SOA from pyrrole and 2-MP are greatly light absorbing in
297 the near UV-range showing a peak of absorbance around 330 nm. The online optical measurements
298 performed with the PAX show strong agreement with the offline measurements. In **Figure 2B**, the
299 $<MAC>_{online,375nm}$ is plotted vs. experiment time, showing significant light absorption for the 2-

MP SOA and the pyrrole SOA and much lower light absorption for the 1-MP SOA. 2-MP shows an average $<MAC>_{online,375}$ of 0.89 ± 0.03 $m^2 g^{-1}$, followed by pyrrole (0.54 ± 0.01 $m^2 g^{-1}$) and 1-MP (0.06 ± 0.01 $m^2 g^{-1}$). In **Figure 2C**, the SSA_{375} is plotted vs. size parameter, where the 2-MP SOA shows the lowest average SSA_{375} of 0.76 ± 0.01, followed by pyrrole (0.80 ± 0.01) and 1-MP (0.97 ± 0.00). The SSA_{375} of the pyrrole SOA from NO_3 oxidation agrees with previously reported results from similar experiments.[14] Therefore, we suggest that the SOA from NO_3 oxidation of 2-MP and pyrrole are strong BrC and show significant light-absorbing capabilities while those from 1-MP show little light-absorbing property and are mostly light scattering. Our calculations of AAE show minimal difference in wavelength dependence in the UV-range (290 – 400 nm) between pyrrole, 1-MP, and 2-MP SOA. However, in the visible range (400 – 600 nm), the SOA derived from the methylpyrroles exhibited stronger wavelength dependence than the pyrrole SOA.

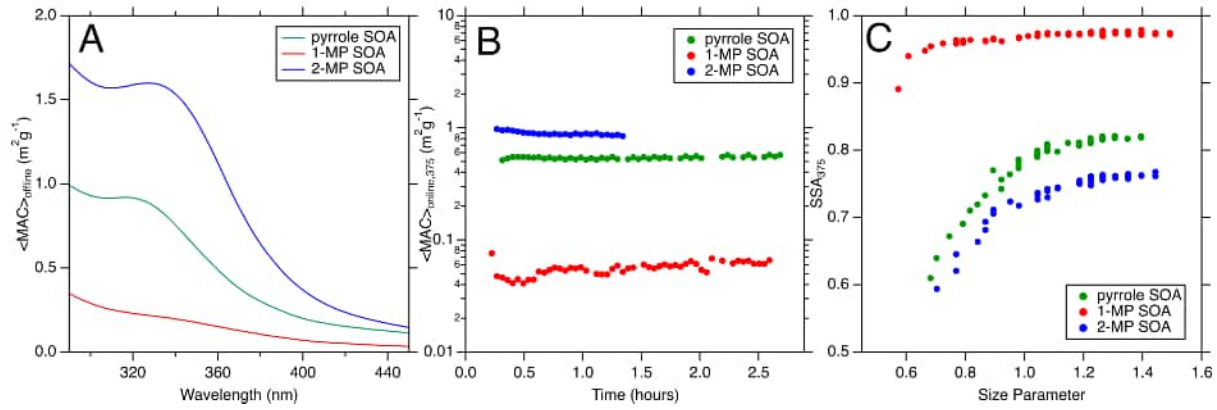

Figure 2. (A): $<MAC>_{offline}$ vs. wavelength (290-450 nm) calculated from UV-Vis and SEMS data of SOA from NO_3 oxidation (with the high-NO_2 condition) of pyrrole (green), 1-MP (red) and 2-MP (blue). (B): $<MAC>_{online,375}$ timeseries and (C): SSA_{375} calculated from the online PAX measurements.

By considering the SOA molecular compositions and optical properties synergistically for all three studied nitrogen-containing heterocyclic VOCs, it is conceivable that their SOA light absorption could be positively related to the abundance of the nitroaromatic products in the SOA. This is consistent with the fact that nitroaromatics have been shown to be strongly light absorbing. In previous studies of NO_3 oxidation of aromatic VOCs, nitroaromatic products generally constituted a significant portion of SOA mass and may have contributed to increased light absorption.[30,32,33,36–39] Although prior work also suggested that organic nitrates could contribute to BrC,[55] their light absorbing ability is likely much weaker. Further, we show that the $<MAC>_{online,375nm}$ measurements from all the NO_3 oxidation experiments (including the duplicate experiments) exhibit clear positive correlations with the ratio of NO^+ and NO_2^+ fragments to total organic ions obtained by the mAMS, which indicate that nitro and nitrate species are likely major contributors to BrC in the SOA (**Figure 3**). Interestingly, the $<MAC>_{online,375nm}$ exhibits a negative correlation with the $CHO_{>1}N^+$ family (**Figure S4**). Assuming that oxygenated organic nitrates ($RONO_2$), as are expected to have formed in the 1-MP system, are more likely to form fragment ions in the $CHO_{>1}N^+$ family (because of the higher oxygen content) than nitroaromatics (RNO_2), this contrast implies that it is the nitroaromatics, rather than organic nitrates, that contribute to the BrC in these systems. In support of this, the LC-DAD-ESI-HR-TOFMS results exhibit strong light absorption at wavelength 320 – 340 nm for dinitropyrrole and 2-methyl-dinitropyrrole (**Figure S2**), consistent with the UV-Vis results. In addition, the TD-DFT calculations show that the predicted UV-Vis spectra of dinitropyrroles (the dominant SOA constituents from pyrrole + NO_3) peak at approximately the same observed UV-Vis peak of the total pyrrole SOA, while organic nitrates show very different spectral shapes with much lower absorbance (by more than two orders of magnitude) under the TD-DFT calculations (**Figure S5**). These pieces of evidence collectively

suggest that nitroaromatics are clearly the dominant, if not the only, BrC chromophores in the SOA formed from NO_3 oxidation of pyrrole and 2-MP.

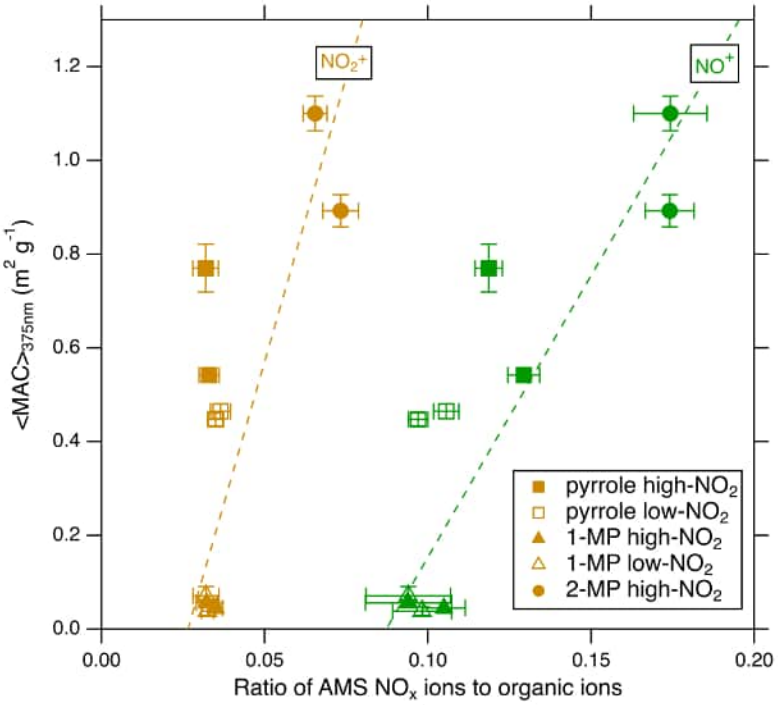

Figure 3. The correlations between $<MAC>_{online,375nm}$ and AMS ion ratios of NO^+ (green) and NO_2^+ (brown) to total organic ions for all the performed experiments. The dashed lines represent the error-weighted Pearson correlation fittings (R = 0.78 for NO_2^+ and 0.81 for NO^+).

Proposed mechanisms for formation of nitroaromatics from NO_3 oxidation of pyrrole and methylpyrroles. After demonstrating that nitroaromatics in the SOA from pyrrole and 2-MP are the dominant constituents and contributors to BrC, it is critical to elucidate their formation mechanisms in the pyrrole and 2-MP systems and explain why nitroaromatics are not largely formed in the 1-MP system. Apparently, a key difference is that both pyrrole and 2-MP are secondary amines with N–H bonds, while 1-MP is a tertiary amine without an N–H bond. Therefore, we propose that the N–H bonds play an important role in the NO_3 oxidation of pyrrole

and 2-MP that led to the substantial formation of nitroaromatics. In **Figure 4**, a mechanism is proposed for the addition of 1, 2, and 3 $–NO_2$ groups to the backbone of pyrrole through NO_3 oxidation. In this mechanism, we propose H-abstraction by NO_3 for pyrrole on the 1-position (H in the N–H bond), followed by a pyrrolyl radical-shift. NO_2 then adds to this radical and a subsequent H-shift would occur to move the hydrogen back to the 1-position and form a nitropyrrole. This initial step is somewhat similar to that proposed for H-abstraction of phenolic species in which nitrophenols are observed.[30–34] The nitropyrroles were not observed in the pyrrole + NO_3 SOA by the IMS-TOF measurements, likely because they are too volatile to partition to the particle phase. But they were indeed dominant gas-phase products, confirmed by the I-CIMS results (**Figure S6**), supporting our proposed mechanism. From here, the mechanism repeats itself beginning with the same H-abstraction on the 1-position by NO_3 for the additions of the second and third $–NO_2$ groups. Through this process, the original aromaticity is retained, facilitating sequential $–NO_2$ addition. For simplicity, the formation of only one dinitropyrrole isomer and one trinitropyrrole isomer are explicitly shown in **Figure 4**, but there could be up to 4 positional dinitropyrrole isomers and 2 trinitropyrrole isomers, depending on how the pyrrolyl radicals shift. In agreement with this, we observe 4 isomers for dinitropyrrole from the extracted ion chromatogram in the LC-DAD-ESI-HR-TOFMS (**Figure S2**). The proposed mechanism is also consistent with the results that higher NO_2 concentrations led to stronger light absorption in the two pyrrole experiments (**Table 1** and **Figure 3**), as higher NO_2 concentrations could enhance formation of dinitro- and trinitro-pyrroles. In the real atmosphere affected by wildfire, NO_2 concentrations have been reported to be as high as ~ 60 ppb, somewhat lower than the experimental conditions in this work.[56] With lower NO_2 concentrations, it is possible that oxygen addition on the pyrrolyl radicals (producing peroxy radicals) could become more competitive in comparison

to NO_2 addition (producing nitropyrroles). However, the likely gas-phase products from peroxy radical chemistry are found to be lower than the nitropyrroles by ~ 3 orders of magnitude with ~ 90 ppb of NO_2 (**Figure S7**), suggesting that the NO_2 addition is the dominant pathway for the pyrrolyl radicals even with ambient-level NO_2 concentrations. These results are highly consistent with prior work on phenoxy radicals from phenol oxidation[57] and *o*-semiquinone radicals from catechol oxidation,[30] both of which suggested dominant NO_2 addition in comparison to oxygen addition.

The mechanism for addition of NO_2 to 2-MP would be analogous to that of pyrrole except that there is a methyl group in the 2-position which might interfere the pyrrolyl radical shift and hence the number of possible positional isomers in comparison to pyrrole. In fact, the results shown in **Figure S2** suggest that there are two major 2-methyl-dinitropyrrole isomers in the 2-MP SOA. It should be noted that there has not been direct measurement-based evidence for the proposed radical or hydrogen shift in the (methyl)pyrrole or the phenolic NO_3 oxidation systems, suggesting that other unrecognized mechanisms cannot be fully ruled out. However, combining all the pieces of evidence discussed above and in the literature,[30–34] this mechanism appears to be a highly likely one.

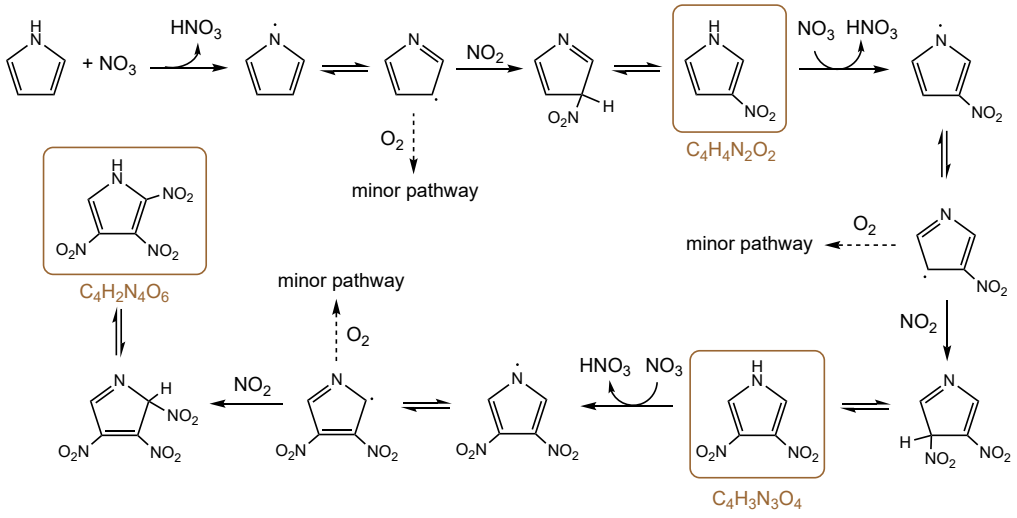

Figure 4. Proposed chemical mechanism for the addition of 1, 2 and 3 NO_2 groups to pyrrole. Only one isomer for each of $C_4H_4N_2O_2$, $C_4H_3N_3O_4$, $C_4H_2N_4O_6$ is shown, but multiple isomers are possibly formed, depending on how the pyrrolyl radicals undergo shift.

In comparison to this mechanism, 1-MP is a tertiary amine and does not contain a N–H bond like pyrrole and 2-MP. Thus, the mechanism shown in **Figure 4** does not work for 1-MP, explaining the absence of dinitro- and trinitro-products in the 1-MP SOA. Based on the measurements discussed above, we also suggest the hydrogen in the N–H bond must be more susceptible to abstraction by NO_3 than other hydrogens on the ring. Instead, in the NO_3 oxidation of 1-MP, we rather observed products with $–NO_3$ and additional oxygen-containing functionality (e.g., –OH). The lack of the secondary amine structure in the backbone of 1-MP may require other mechanisms to occur for 1-MP such as NO_3 addition to the double bond. A tentative mechanism is proposed in **Figure S8**, which may explain some of the observed 1-MP gas-phase and SOA constituents. Particularly, the dominant gas-phase product, $C_5H_7NO_2$ (**Figure S6**) is likely formed through nitrooxy alkoxy radical bond scission and NO_2 removal.[58] The analogous product in the pyrrole system ($C_4H_5NO_2$) appears to be much smaller (**Figure S6**), again supporting that NO_3 oxidation of pyrrole is mainly through H-abstraction. For 1-MP, the breaking of aromaticity through the addition of $–NO_3$ and –OH functional groups ultimately lead to decreased light absorption in the SOA. Conversely, the retention of aromaticity and the addition of a strong electron-withdrawing group, $–NO_2$, increases the strong light absorption of the pyrrole and 2-MP SOA. The proposed mechanisms highlight the importance of secondary amines as key structures in pyrrole and methylpyrroles to form BrC chromophores.

Atmospheric Implications

In this study, we have demonstrated that small differences in the structures of pyrrole and its methyl derivatives have significant implications for the optical properties of their SOA from NO_3 oxidation. The NO_3 oxidation of 2-MP and pyrrole led to SOA compositions which were almost entirely caused by products resulting from the addition of two or three $–NO_2$ groups. These nitroaromatic products resulted in the strong light absorption of the SOA from 2-MP and pyrrole. To understand the significance of the pyrrole and methylpyrroles on SOA mass concentration and BrC light absorption from atmospheric biomass burning of different fuels, we estimate the SOA formation potential (SOA_{pot}, g of SOA potentially formed per kg of fuel) and absorption cross-section emission factor (EF_{abs}, m^2 of absorption per kg of fuel) for pyrrole, 2-MP, and several other relevant VOC oxidation systems (i.e., phenolic VOC + NO_3 and toluene + OH/NO_x).[14] The estimations are based on emission factors (EF) from typical biomass burning fuels reported in previous work,[5,8,9] SOA yields from previous laboratory oxidation studies,[35,59] and the reported <MAC> results for the corresponding SOA in literature:[35,60]

$$SOA_{pot,i} = EF_i \times Y_{SOA,i} \quad (7)$$

$$EF_{abs,i} = SOA_{pot,i} \times < MAC >_i \quad (8)$$

where $Y_{SOA,i}$ is the estimated SOA yield for a VOC species, *i*. The details are shown in **Tables S3–S5**. For the VOCs whose SOA yields or <MAC> values are unknown, we use results from a similar VOC in the same category as a reasonable approximate. From these calculations, we compare the SOA_{pot} and EF_{abs} between the summed SOA from NO_3 oxidation of pyrrole and 2-MP with total phenolic + NO_3 SOA and toluene photooxidation SOA. In a recent study, Palm et al. reported that phenolic SOA may contribute to 29 ± 15% of biomass burning BrC during daytime and underscored the importance to study nighttime processes of biomass burning emissions.[61] Kodros

et al. also pointed out that nighttime oxidation of biomass burning emissions may be an overlooked source of oxidized organic aerosols.[62] Here, we estimate that the total SOA_{pot} from NO_3 oxidation of pyrrole and 2-MP may be 119 – 189% of that from NO_3 oxidation of phenolic VOCs and 52 – 277% of that from toluene photooxidation. In addition, the total EF_{abs} of pyrrole and 2-MP SOA is 25 – 49% of that for the phenolic + NO_3 SOA and 36 – 170% of that for toluene photooxidation SOA. The large variations in these comparisons are due to strong fuel dependence of the VOC emission factors. Although SOA yields and <MAC> results were obtained from different studies under different experimental conditions, and thus some uncertainties are expected, these findings clearly demonstrate that the SOA from nighttime oxidation of pyrrole and 2-MP will significantly contribute to SOA mass concentration and light absorption in biomass burning derived aerosols. Therefore, their oxidation chemistry and contribution to SOA and BrC need to be implemented in air quality and climate models. The SOA and BrC formation from nighttime oxidation of nitrogen-containing heterocyclic VOCs have been understudied. This study filled the knowledge gap and demonstrated that small differences in chemical structure for these nitrogen-containing heterocyclic VOCs have significant impacts on the chemical composition and light-absorption of SOA.

Associated Contents

Supporting Information

Additional experimental details and methods, TD-DFT calculation details, fuel-based SOA formation potential and absorption cross-section emission factor calculations, supporting mass spectra, chromatograms, and mechanisms.

Author Information

Corresponding Authors

E-mail address: haofei.zhang@ucr.edu (H. Zhang).

Notes

The authors declare no competing financial interest.

Acknowledgements

This work was supported by National Science Foundation (AGS-1953905) and USDA NIFA Hatch Accession No. 1015963 (Project No. CA-R-ENS-5072-H). The LC-DAD-ESI-Q-TOFMS analysis at Analytical Chemistry Instrumentation Facility (ACIF) was supported by NSF (CHE-0541848). Computations were performed using the computer clusters and data storage resources of the UCR HPCC, which were funded by grants from NSF (MRI-1429826) and NIH (1S10OD016290-01A1). We gratefully acknowledge use of the PAX instrument acquired with support from NSF AGS-1454374.

References

(1) Di Virgilio, G.; Evans, J. P.; Blake, S. A. P.; Armstrong, M.; Dowdy, A. J.; Sharples, J.; McRae, R. Climate Change Increases the Potential for Extreme Wildfires. *Geophysical Research Letters* **2019**, *46* (14), 8517–8526. https://doi.org/10.1029/2019GL083699.

(2) Dennison, P. E.; Brewer, S. C.; Arnold, J. D.; Moritz, M. A. Large Wildfire Trends in the Western United States, 1984-2011. *Geophys. Res. Lett.* **2014**, *41* (8), 2928–2933. https://doi.org/10.1002/2014GL059576.

(3) Crutzen, P. J.; Andreae, M. O. Biomass Burning in the Tropics: Impact on Atmospheric Chemistry and Biogeochemical Cycles. *Science* **1990**, *250* (4988), 1669–1678. https://doi.org/10.1126/science.250.4988.1669.

(4) Pope, C. A.; Dockery, D. W. Health Effects of Fine Particulate Air Pollution: Lines That Connect. *Journal of the Air & Waste Management Association* **2006**, *56* (6), 709–742. https://doi.org/10.1080/10473289.2006.10464485.

(5) Hatch, L. E.; Luo, W.; Pankow, J. F.; Yokelson, R. J.; Stockwell, C. E.; Barsanti, K. C. Identification and Quantification of Gaseous Organic Compounds Emitted from Biomass Burning Using Two-Dimensional Gas Chromatography–Time-of-Flight Mass Spectrometry. *Atmos. Chem. Phys.* **2015**, *15* (4), 1865–1899. https://doi.org/10.5194/acp-15-1865-2015.

(6) Koss, A. R.; Sekimoto, K.; Gilman, J. B.; Selimovic, V.; Coggon, M. M.; Zarzana, K. J.; Yuan, B.; Lerner, B. M.; Brown, S. S.; Jimenez, J. L.; Krechmer, J.; Roberts, J. M.; Warneke, C.; Yokelson, R. J.; de Gouw, J. Non-Methane Organic Gas Emissions from Biomass Burning: Identification, Quantification, and Emission Factors from PTR-ToF during the FIREX 2016 Laboratory Experiment. *Atmos. Chem. Phys.* **2018**, *18* (5), 3299–3319. https://doi.org/10.5194/acp-18-3299-2018.

(7) Hatch, L. E.; Yokelson, R. J.; Stockwell, C. E.; Veres, P. R.; Simpson, I. J.; Blake, D. R.; Orlando, J. J.; Barsanti, K. C. Multi-Instrument Comparison and Compilation of Non-Methane Organic Gas Emissions from Biomass Burning and Implications for Smoke-Derived Secondary Organic Aerosol Precursors. *Atmos. Chem. Phys.* **2017**, *17* (2), 1471–1489. https://doi.org/10.5194/acp-17-1471-2017.

(8) Oros, D. R.; Simoneit, B. R. T. Identification and Emission Factors of Molecular Tracers in Organic Aerosols from Biomass Burning Part 1. Temperate Climate Conifers. *Applied Geochemistry* **2001**, *16* (13), 1513–1544. https://doi.org/10.1016/S0883-2927(01)00021-X.

(9) Fine, P. M.; Cass, G. R.; Simoneit, B. R. T. Chemical Characterization of Fine Particle Emissions from the Fireplace Combustion of Wood Types Grown in the Midwestern and Western United States. *Environmental Engineering Science* **2004**, *21* (3), 387–409. https://doi.org/10.1089/109287504323067021.

(10) Brown, S. S.; Stutz, J. Nighttime Radical Observations and Chemistry. *Chem. Soc. Rev.* **2012**, *41* (19), 6405. https://doi.org/10.1039/c2cs35181a.

(11) Stockwell, C. E.; Yokelson, R. J.; Kreidenweis, S. M.; Robinson, A. L.; DeMott, P. J.; Sullivan, R. C.; Reardon, J.; Ryan, K. C.; Griffith, D. W. T.; Stevens, L. Trace Gas Emissions from Combustion of Peat, Crop Residue, Domestic Biofuels, Grasses, and Other Fuels: Configuration and Fourier Transform Infrared (FTIR) Component of the Fourth Fire Lab at

Missoula Experiment (FLAME-4). *Atmos. Chem. Phys.* **2014**, *14* (18), 9727–9754. https://doi.org/10.5194/acp-14-9727-2014.

(12) Bluvshtein, N.; Lin, P.; Flores, J. M.; Segev, L.; Mazar, Y.; Tas, E.; Snider, G.; Weagle, C.; Brown, S. S.; Laskin, A.; Rudich, Y. Broadband Optical Properties of Biomass-Burning Aerosol and Identification of Brown Carbon Chromophores: OPTICAL AND CHEMICAL PROPERTIES OF BROWN CARBON AEROSOLS. *J. Geophys. Res. Atmos.* **2017**, *122* (10), 5441–5456. https://doi.org/10.1002/2016JD026230.

(13) Decker, Z. C. J.; Robinson, M. A.; Barsanti, K. C.; Bourgeois, I.; Coggon, M. M.; DiGangi, J. P.; Diskin, G. S.; Flocke, F. M.; Franchin, A.; Fredrickson, C. D.; Gkatzelis, G. I.; Hall, S. R.; Halliday, H.; Holmes, C. D.; Huey, L. G.; Lee, Y. R.; Lindaas, J.; Middlebrook, A. M.; Montzka, D. D.; Moore, R.; Neuman, J. A.; Nowak, J. B.; Palm, B. B.; Peischl, J.; Piel, F.; Rickly, P. S.; Rollins, A. W.; Ryerson, T. B.; Schwantes, R. H.; Sekimoto, K.; Thornhill, L.; Thornton, J. A.; Tyndall, G. S.; Ullmann, K.; Van Rooy, P.; Veres, P. R.; Warneke, C.; Washenfelder, R. A.; Weinheimer, A. J.; Wiggins, E.; Winstead, E.; Wisthaler, A.; Womack, C.; Brown, S. S. Nighttime and Daytime Dark Oxidation Chemistry in Wildfire Plumes: An Observation and Model Analysis of FIREX-AQ Aircraft Data. *Atmos. Chem. Phys.* **2021**, *21* (21), 16293–16317. https://doi.org/10.5194/acp-21-16293-2021.

(14) Jiang, H.; Frie, A. L.; Lavi, A.; Chen, J. Y.; Zhang, H.; Bahreini, R.; Lin, Y.-H. Brown Carbon Formation from Nighttime Chemistry of Unsaturated Heterocyclic Volatile Organic Compounds. *Environ. Sci. Technol. Lett.* **2019**, *6* (3), 184–190. https://doi.org/10.1021/acs.estlett.9b00017.

(15) Lin, P.; Fleming, L. T.; Nizkorodov, S. A.; Laskin, J.; Laskin, A. Comprehensive Molecular Characterization of Atmospheric Brown Carbon by High Resolution Mass Spectrometry with Electrospray and Atmospheric Pressure Photoionization. *Anal. Chem.* **2018**, *90* (21), 12493–12502. https://doi.org/10.1021/acs.analchem.8b02177.

(16) Lin, P.; Bluvshtein, N.; Rudich, Y.; Nizkorodov, S. A.; Laskin, J.; Laskin, A. Molecular Chemistry of Atmospheric Brown Carbon Inferred from a Nationwide Biomass Burning Event. *Environ. Sci. Technol.* **2017**, *51* (20), 11561–11570. https://doi.org/10.1021/acs.est.7b02276.

(17) Lin, P.; Liu, J.; Shilling, J. E.; Kathmann, S. M.; Laskin, J.; Laskin, A. Molecular Characterization of Brown Carbon (BrC) Chromophores in Secondary Organic Aerosol Generated from Photo-Oxidation of Toluene. *Phys. Chem. Chem. Phys.* **2015**, *17* (36), 23312–23325. https://doi.org/10.1039/C5CP02563J.

(18) Joo, T.; Rivera-Rios, J. C.; Takeuchi, M.; Alvarado, M. J.; Ng, N. L. Secondary Organic Aerosol Formation from Reaction of 3-Methylfuran with Nitrate Radicals. *ACS Earth Space Chem.* **2019**, *3* (6), 922–934. https://doi.org/10.1021/acsearthspacechem.9b00068.

(19) Jiang, J.; Carter, W. P. L.; Cocker, D. R.; Barsanti, K. C. Development and Evaluation of a Detailed Mechanism for Gas-Phase Atmospheric Reactions of Furans. *ACS Earth Space Chem.* **2020**, *4* (8), 1254–1268. https://doi.org/10.1021/acsearthspacechem.0c00058.

(20) Li, M.; Liu, Y.; Wang, L. Gas-Phase Ozonolysis of Furans, Methylfurans, and Dimethylfurans in the Atmosphere. *Phys. Chem. Chem. Phys.* **2018**, *20* (38), 24735–24743. https://doi.org/10.1039/C8CP04947E.

(21) Tekle-Röttering, A.; Lim, S.; Reisz, E.; Lutze, H. V.; Abdighahroudi, M. S.; Willach, S.; Schmidt, W.; Tentscher, P. R.; Rentsch, D.; McArdell, C. S.; Schmidt, T. C.; von Gunten, U. Reactions of Pyrrole, Imidazole, and Pyrazole with Ozone: Kinetics and Mechanisms. *Environ. Sci.: Water Res. Technol.* **2020**, *6* (4), 976–992. https://doi.org/10.1039/C9EW01078E.

(22) Atkinson, Roger.; Aschmann, S. M.; Winer, A. M.; Carter, W. P. L. Rate Constants for the Gas-Phase Reactions of Nitrate Radicals with Furan, Thiophene, and Pyrrole at 295 +/- 1 K and Atmospheric Pressure. *Environ. Sci. Technol.* **1985**, *19* (1), 87–90. https://doi.org/10.1021/es00131a010.

(23) Cabañas, B.; Baeza, M. T.; Salgado, S.; Martín, P.; Taccone, R.; Martínez, E. Oxidation of Heterocycles in the Atmosphere: Kinetic Study of Their Reactions with NO3 Radical. *J. Phys. Chem. A* **2004**, *108* (49), 10818–10823. https://doi.org/10.1021/jp046524t.

(24) Fry, J. L.; Draper, D. C.; Barsanti, K. C.; Smith, J. N.; Ortega, J.; Winkler, P. M.; Lawler, M. J.; Brown, S. S.; Edwards, P. M.; Cohen, R. C.; Lee, L. Secondary Organic Aerosol Formation and Organic Nitrate Yield from NO_3 Oxidation of Biogenic Hydrocarbons. *Environ. Sci. Technol.* **2014**, *48* (20), 11944–11953. https://doi.org/10.1021/es502204x.

(25) Fry, J. L.; Kiendler-Scharr, A.; Rollins, A. W.; Brauers, T.; Brown, S. S.; Dorn, H.-P.; Dubé, W. P.; Fuchs, H.; Mensah, A.; Rohrer, F.; Tillmann, R.; Wahner, A.; Wooldridge, P. J.; Cohen, R. C. SOA from Limonene: Role of NO3 in Its Generation and Degradation. *Atmos. Chem. Phys.* **2011**, *11* (8), 3879–3894. https://doi.org/10.5194/acp-11-3879-2011.

(26) Fry, J. L.; Kiendler-Scharr, A.; Rollins, A. W.; Wooldridge, P. J.; Brown, S. S.; Fuchs, H.; Dubé, W.; Mensah, A.; dal Maso, M.; Tillmann, R.; Dorn, H.-P.; Brauers, T.; Cohen, R. C. Organic Nitrate and Secondary Organic Aerosol Yield from NO3 Oxidation of β-Pinene Evaluated Using a Gas-Phase Kinetics/Aerosol Partitioning Model. *Atmos. Chem. Phys.* **2009**, *9* (4), 1431–1449. https://doi.org/10.5194/acp-9-1431-2009.

(27) Rollins, A. W.; Fry, J. L.; Hunter, J. F.; Kroll, J. H.; Worsnop, D. R.; Singaram, S. W.; Cohen, R. C. Elemental Analysis of Aerosol Organic Nitrates with Electron Ionization High-Resolution Mass Spectrometry. *Atmos. Meas. Tech.* **2010**, *3* (1), 301–310. https://doi.org/10.5194/amt-3-301-2010.

(28) Rollins, A. W.; Pusede, S.; Wooldridge, P.; Min, K.-E.; Gentner, D. R.; Goldstein, A. H.; Liu, S.; Day, D. A.; Russell, L. M.; Rubitschun, C. L.; Surratt, J. D.; Cohen, R. C. Gas/Particle Partitioning of Total Alkyl Nitrates Observed with TD-LIF in Bakersfield: RONO2 Phase Partitioning. *J. Geophys. Res. Atmos.* **2013**, *118* (12), 6651–6662. https://doi.org/10.1002/jgrd.50522.

(29) Nah, T.; Sanchez, J.; Boyd, C. M.; Ng, N. L. Photochemical Aging of α-Pinene and β-Pinene Secondary Organic Aerosol Formed from Nitrate Radical Oxidation. *Environ. Sci. Technol.* **2016**, *50* (1), 222–231. https://doi.org/10.1021/acs.est.5b04594.

(30) Finewax, Z.; de Gouw, J. A.; Ziemann, P. J. Identification and Quantification of 4-Nitrocatechol Formed from OH and NO3 Radical-Initiated Reactions of Catechol in Air in the Presence of NOx: Implications for Secondary Organic Aerosol Formation from Biomass Burning. *Environ. Sci. Technol.* **2018**, *52* (4), 1981–1989. https://doi.org/10.1021/acs.est.7b05864.

(31) Finewax, Z.; de Gouw, J. A.; Ziemann, P. J. Products and Secondary Organic Aerosol Yields from the OH and NO3 Radical-Initiated Oxidation of Resorcinol. *ACS Earth Space Chem.* **2019**, *3* (7), 1248–1259. https://doi.org/10.1021/acsearthspacechem.9b00112.
(32) Vidović, K.; Lašič Jurković, D.; Šala, M.; Kroflič, A.; Grgić, I. Nighttime Aqueous-Phase Formation of Nitrocatechols in the Atmospheric Condensed Phase. *Environ. Sci. Technol.* **2018**, *52* (17), 9722–9730. https://doi.org/10.1021/acs.est.8b01161.
(33) Bolzacchini, E.; Bruschi, M.; Hjorth, J.; Meinardi, S.; Orlandi, M.; Rindone, B.; Rosenbohm, E. Gas-Phase Reaction of Phenol with NO_3. *Environ. Sci. Technol.* **2001**, *35* (9), 1791–1797. https://doi.org/10.1021/es001290m.
(34) Kroflič, A.; Grilc, M.; Grgić, I. Unraveling Pathways of Guaiacol Nitration in Atmospheric Waters: Nitrite, A Source of Reactive Nitronium Ion in the Atmosphere. *Environ. Sci. Technol.* **2015**, *49* (15), 9150–9158. https://doi.org/10.1021/acs.est.5b01811.
(35) Mayorga, R. J.; Zhao, Z.; Zhang, H. Formation of Secondary Organic Aerosol from Nitrate Radical Oxidation of Phenolic VOCs: Implications for Nitration Mechanisms and Brown Carbon Formation. *Atmospheric Environment* **2021**, *244*, 117910. https://doi.org/10.1016/j.atmosenv.2020.117910.
(36) Frka, S.; Šala, M.; Kroflič, A.; Huš, M.; Čusak, A.; Grgić, I. Quantum Chemical Calculations Resolved Identification of Methylnitrocatechols in Atmospheric Aerosols. *Environ. Sci. Technol.* **2016**, *50* (11), 5526–5535. https://doi.org/10.1021/acs.est.6b00823.
(37) Kitanovski, Z.; Čusak, A.; Grgić, I.; Claeys, M. Chemical Characterization of the Main Products Formed through Aqueous-Phase Photonitration of Guaiacol. *Atmos. Meas. Tech.* **2014**, *7* (8), 2457–2470. https://doi.org/10.5194/amt-7-2457-2014.
(38) Vidović, K.; Kroflič, A.; Šala, M.; Grgić, I. Aqueous-Phase Brown Carbon Formation from Aromatic Precursors under Sunlight Conditions. *Atmosphere* **2020**, *11* (2), 131. https://doi.org/10.3390/atmos11020131.
(39) Yuan, B.; Liggio, J.; Wentzell, J.; Li, S.-M.; Stark, H.; Roberts, J. M.; Gilman, J.; Lerner, B.; Warneke, C.; Li, R.; Leithead, A.; Osthoff, H. D.; Wild, R.; Brown, S. S.; de Gouw, J. A. Secondary Formation of Nitrated Phenols: Insights from Observations during the Uintah Basin Winter Ozone Study (UBWOS) 2014. *Atmos. Chem. Phys.* **2016**, *16* (4), 2139–2153. https://doi.org/10.5194/acp-16-2139-2016.
(40) Singh, H. B.; Anderson, B. E.; Brune, W. H.; Cai, C.; Cohen, R. C.; Crawford, J. H.; Cubison, M. J.; Czech, E. P.; Emmons, L.; Fuelberg, H. E. Pollution Influences on Atmospheric Composition and Chemistry at High Northern Latitudes: Boreal and California Forest Fire Emissions. *Atmospheric Environment* **2010**, *44* (36), 4553–4564. https://doi.org/10.1016/j.atmosenv.2010.08.026.
(41) Zhao, Z.; Zhang, W.; Alexander, T.; Zhang, X.; Martin, D. B. C.; Zhang, H. Isolating α-Pinene Ozonolysis Pathways Reveals New Insights into Peroxy Radical Chemistry and Secondary Organic Aerosol Formation. *Environ. Sci. Technol.* **2021**, *55* (10), 6700–6709. https://doi.org/10.1021/acs.est.1c02107.
(42) Zhang, X.; Zhang, H.; Xu, W.; Wu, X.; Tyndall, G. S.; Orlando, J. J.; Jayne, J. T.; Worsnop, D. R.; Canagaratna, M. R. Molecular Characterization of Alkyl Nitrates in Atmospheric Aerosols by Ion Mobility Mass Spectrometry. *Atmos. Meas. Tech.* **2019**, *12* (10), 5535–5545. https://doi.org/10.5194/amt-12-5535-2019.

(43) Zhao, Z.; Yang, X.; Lee, J.; Tolentino, R.; Mayorga, R.; Zhang, W.; Zhang, H. Diverse Reactions in Highly Functionalized Organic Aerosols during Thermal Desorption. *ACS Earth Space Chem.* **2020**, *4* (2), 283–296. https://doi.org/10.1021/acsearthspacechem.9b00312.
(44) Zhao, Z.; Le, C.; Xu, Q.; Peng, W.; Jiang, H.; Lin, Y.-H.; Cocker, D. R.; Zhang, H. Compositional Evolution of Secondary Organic Aerosol as Temperature and Relative Humidity Cycle in Atmospherically Relevant Ranges. *ACS Earth Space Chem.* **2019**, *3* (11), 2549–2558. https://doi.org/10.1021/acsearthspacechem.9b00232.
(45) Bahreini, R.; Keywood, M. D.; Ng, N. L.; Varutbangkul, V.; Gao, S.; Flagan, R. C.; Seinfeld, J. H.; Worsnop, D. R.; Jimenez, J. L. Measurements of Secondary Organic Aerosol from Oxidation of Cycloalkenes, Terpenes, and m-Xylene Using an Aerodyne Aerosol Mass Spectrometer. *Environ. Sci. Technol.* **2005**, *39* (15), 5674–5688. https://doi.org/10.1021/es048061a.
(46) Cui, Y.; Frie, A. L.; Dingle, J. H.; Zimmerman, S.; Frausto-Vicencio, I.; Hopkins, F.; Bahreini, R. Influence of Ammonia and Relative Humidity on the Formation and Composition of Secondary Brown Carbon from Oxidation of 1-Methylnaphthalene and Longifolene. *ACS Earth Space Chem.* **2021**, *5* (4), 858–869. https://doi.org/10.1021/acsearthspacechem.0c00353.
(47) DeCarlo, P. F.; Slowik, J. G.; Worsnop, D. R.; Davidovits, P.; Jimenez, J. L. Particle Morphology and Density Characterization by Combined Mobility and Aerodynamic Diameter Measurements. Part 1: Theory. *Aerosol Science and Technology* **2004**, *38* (12), 1185–1205. https://doi.org/10.1080/027868290903907.
(48) Bahreini, R.; Middlebrook, A. M.; Brock, C. A.; de Gouw, J. A.; McKeen, S. A.; Williams, L. R.; Daumit, K. E.; Lambe, A. T.; Massoli, P.; Canagaratna, M. R.; Ahmadov, R.; Carrasquillo, A. J.; Cross, E. S.; Ervens, B.; Holloway, J. S.; Hunter, J. F.; Onasch, T. B.; Pollack, I. B.; Roberts, J. M.; Ryerson, T. B.; Warneke, C.; Davidovits, P.; Worsnop, D. R.; Kroll, J. H. Mass Spectral Analysis of Organic Aerosol Formed Downwind of the Deepwater Horizon Oil Spill: Field Studies and Laboratory Confirmations. *Environ. Sci. Technol.* **2012**, *46* (15), 8025–8034. https://doi.org/10.1021/es301691k.
(49) Bloss, C.; Wagner, V.; Jenkin, M. E.; Volkamer, R.; Bloss, W. J.; Lee, J. D.; Heard, D. E.; Wirtz, K.; Martin-Reviejo, M.; Rea, G.; Wenger, J. C.; Pilling, M. J. Development of a Detailed Chemical Mechanism (MCMv3.1) for the Atmospheric Oxidation of Aromatic Hydrocarbons. *Atmos. Chem. Phys.* **2005**, *5* (3), 641–664. https://doi.org/10.5194/acp-5-641-2005.
(50) Fry, J. L.; Draper, D. C.; Barsanti, K. C.; Smith, J. N.; Ortega, J.; Winkler, P. M.; Lawler, M. J.; Brown, S. S.; Edwards, P. M.; Cohen, R. C.; Lee, L. Secondary Organic Aerosol Formation and Organic Nitrate Yield from NO3 Oxidation of Biogenic Hydrocarbons. *Environ. Sci. Technol.* **2014**, *48* (20), 11944–11953. https://doi.org/10.1021/es502204x.
(51) Chen, J. Y.; Rodriguez, E.; Jiang, H.; Chen, K.; Frie, A.; Zhang, H.; Bahreini, R.; Lin, Y.-H. Time-Dependent Density Functional Theory Investigation of the UV–Vis Spectra of Organonitrogen Chromophores in Brown Carbon. *ACS Earth Space Chem.* **2020**, *4* (2), 311–320. https://doi.org/10.1021/acsearthspacechem.9b00328.
(52) Zhang, X.; Krechmer, J. E.; Groessl, M.; Xu, W.; Graf, S.; Cubison, M.; Jayne, J. T.; Jimenez, J. L.; Worsnop, D. R.; Canagaratna, M. R. A Novel Framework for Molecular

Characterization of Atmospherically Relevantorganic Compounds Based on Collision Cross Section and Mass-to-Charge Ratio. *Atmos. Chem. Phys.* **2016**, *16* (20), 12945–12959. https://doi.org/10.5194/acp-16-12945-2016.

(53) De Haan, D. O.; Jansen, K.; Rynaski, A. D.; Sueme, W. R. P.; Torkelson, A. K.; Czer, E. T.; Kim, A. K.; Rafla, M. A.; De Haan, A. C.; Tolbert, M. A. Brown Carbon Production by Aqueous-Phase Interactions of Glyoxal and SO2. *Environ. Sci. Technol.* **2020**, *54* (8), 4781–4789. https://doi.org/10.1021/acs.est.9b07852.

(54) Lopez-Hilfiker, F. D.; Pospisilova, V.; Huang, W.; Kalberer, M.; Mohr, C.; Stefenelli, G.; Thornton, J. A.; Baltensperger, U.; Prevot, A. S. H.; Slowik, J. G. An Extractive Electrospray Ionization Time-of-Flight Mass Spectrometer (EESI-TOF) for Online Measurement of Atmospheric Aerosol Particles. *Atmos. Meas. Tech.* **2019**, *12* (9), 4867–4886. https://doi.org/10.5194/amt-12-4867-2019.

(55) Liu, S.; Shilling, J. E.; Song, C.; Hiranuma, N.; Zaveri, R. A.; Russell, L. M. Hydrolysis of Organonitrate Functional Groups in Aerosol Particles. *Aerosol Science and Technology* **2012**, *46* (12), 1359–1369. https://doi.org/10.1080/02786826.2012.716175.

(56) Bourgeois, I.; Peischl, J.; Neuman, J. A.; Brown, S. S.; Allen, H. M.; Campuzano-Jost, P.; Coggon, M. M.; DiGangi, J. P.; Diskin, G. S.; Gilman, J. B.; Gkatzelis, G. I.; Guo, H.; Halliday, H.; Hanisco, T. F.; Holmes, C. D.; Huey, L. G.; Jimenez, J. L.; Lamplugh, A. D.; Lee, Y. R.; Lindaas, J.; Moore, R. H.; Nowak, J. B.; Pagonis, D.; Rickly, P. S.; Robinson, M. A.; Rollins, A. W.; Selimovic, V.; St. Clair, J. M.; Tanner, D.; Vasquez, K. T.; Veres, P. R.; Warneke, C.; Wennberg, P. O.; Washenfelder, R. A.; Wiggins, E. B.; Womack, C. C.; Xu, L.; Zarzana, K. J.; Ryerson, T. B. *Comparison of Airborne Measurements of NO, NO2;, HONO, NOy; and CO during FIREX-AQ*; preprint; Gases/In Situ Measurement/Instruments and Platforms, 2022. https://doi.org/10.5194/amt-2021-432.

(57) Platz, J.; Nielsen, O. J.; Wallington, T. J.; Ball, J. C.; Hurley, M. D.; Straccia, A. M.; Schneider, W. F.; Sehested, J. Atmospheric Chemistry of the Phenoxy Radical, C6H5O(•): UV Spectrum and Kinetics of Its Reaction with NO, NO2 , and O2. *J. Phys. Chem. A* **1998**, *102* (41), 7964–7974. https://doi.org/10.1021/jp982221l.

(58) Kurtén, T.; Møller, K. H.; Nguyen, T. B.; Schwantes, R. H.; Misztal, P. K.; Su, L.; Wennberg, P. O.; Fry, J. L.; Kjaergaard, H. G. Alkoxy Radical Bond Scissions Explain the Anomalously Low Secondary Organic Aerosol and Organonitrate Yields From α-Pinene + NO3. *J. Phys. Chem. Lett.* **2017**, *8* (13), 2826–2834. https://doi.org/10.1021/acs.jpclett.7b01038.

(59) Jiang, H.; Jang, M.; Yu, Z. Dithiothreitol Activity by Particulate Oxidizers of SOA Produced from Photooxidation of Hydrocarbons under Varied NOx Levels. *Atmos. Chem. Phys.* **2017**, *17* (16), 9965–9977. https://doi.org/10.5194/acp-17-9965-2017.

(60) Liu, J.; Lin, P.; Laskin, A.; Laskin, J.; Kathmann, S. M.; Wise, M.; Caylor, R.; Imholt, F.; Selimovic, V.; Shilling, J. E. Optical Properties and Aging of Light-Absorbing Secondary Organic Aerosol. *Atmos. Chem. Phys.* **2016**, *16* (19), 12815–12827. https://doi.org/10.5194/acp-16-12815-2016.

(61) Palm, B. B.; Peng, Q.; Fredrickson, C. D.; Lee, B. H.; Garofalo, L. A.; Pothier, M. A.; Kreidenweis, S. M.; Farmer, D. K.; Pokhrel, R. P.; Shen, Y.; Murphy, S. M.; Permar, W.; Hu, L.; Campos, T. L.; Hall, S. R.; Ullmann, K.; Zhang, X.; Flocke, F.; Fischer, E. V.; Thornton, J. A. Quantification of Organic Aerosol and Brown Carbon Evolution in Fresh Wildfire

Plumes. *Proc. Natl. Acad. Sci. U.S.A.* **2020**, *117* (47), 29469–29477. https://doi.org/10.1073/pnas.2012218117.

(62) Kodros, J. K.; Papanastasiou, D. K.; Paglione, M.; Masiol, M.; Squizzato, S.; Florou, K.; Skyllakou, K.; Kaltsonoudis, C.; Nenes, A.; Pandis, S. N. Rapid Dark Aging of Biomass Burning as an Overlooked Source of Oxidized Organic Aerosol. *Proc. Natl. Acad. Sci. U.S.A.* **2020**, *117* (52), 33028–33033. https://doi.org/10.1073/pnas.2010365117.